Raman Spectroscopic Study of Effect of Steam and Carbon Dioxide Activation on Microstructure of Polyacrylonitrile-Based Activated Carbon Fabrics

TSE-HAO KO,[1] WEN-SHYONG KUO,[2] CHUNG-HUA HU[1]

[1] Department of Materials Science, Carbon Fibers Laboratory, Feng Chia University, Taichung, Taiwan, Republic of China

[2] Department of Aeronautical Engineering, Feng Chia University, Taichung, Taiwan, Republic of China

Received 20 November 1999; accepted 15 September 2000

ABSTRACT: This work presents the different effects of steam and carbon dioxide activation on the microstructure of an oxidized polyacrylonitrile (PAN) fabric. An investigation was conducted on a series of carbonized fabrics and two series of activated carbon fabrics. The fabrics were activated by steam and carbon dioxide using heat-treatment temperatures of 900–1100°C. Steam and carbon dioxide developed the microstructure initially present in the PAN-based activated carbon fabrics, but with different effects. These fabrics in the form of fabric and powder were examined by X-ray diffraction and Raman spectrometry. This study indicated that carbon dioxide only reacted with the crystalline edges or the irregular carbon on the fiber surface and that the inside structure of the fibers was not greatly affected. When the fabrics were activated using steam, water molecules reacted not only on the fiber surface but also with the carbon at the crystal edge and/or the nonregular carbon in the fibers, which led to communicating pore structures on the surface and in the inner portions of the fiber. This activation also promoted the denitrogenation reactions. Because of these structures and reactions, the activated carbon fabrics, which were activated by steam, had the highest stacking height for carbon layer planes (L_c), the highest number of layer planes (L_c/d_{002}), the highest oxygen content, the largest crystal size (L_a), and the highest density over the other samples. © 2001 John Wiley & Sons, Inc. J Appl Polym Sci 81: 1090–1099, 2001

Key words: Raman spectrometry; polyacrylonitrile; activated carbon fabrics; steam; carbon dioxide

INTRODUCTION

Activated carbons are widely used for purification and separation. These carbons are common in granulated, powdered, or molded form. Recently, scientists have paid much attention to activated carbon fibers (ACFs) because of their novel adsorption properties. These ACFs have unique characteristics compared with granular or powder activated carbons. Because of their thin fiber shape, ACFs have fast intraparticle adsorption kinetics compared with activated carbon commonly used in gas-phase and aqueous-phase adsorption.[1,2] Viscose rayon, pitch fiber, phenolic fiber, and polyacrylonitrile (PAN) fiber are raw materials that produce high surface area ACFs.[3–7] Because of the nitrogen atoms contained

Correspondence to: T.-H. Ko (thko@fcu.edu.tw).

Contract grant sponsor: National Science Council; contract grant number: NSC 88-2216-E-035-001.

Journal of Applied Polymer Science, Vol. 81, 1090–1099 (2001)

Table I X-Ray Diffraction Results of Carbon Fabrics and Activated Carbon Fabrics

		Sample Form					
		Fabric			Powder		
Sample Code	Activation	d_{002} (nm)	L_c (nm)	L_c/d_{002}	d_{002} (nm)	L_c (nm)	L_c/d_{002}
B900	None	0.351	1.557	4.4	0.351	1.462	4.2
B950		0.352	1.465	4.2	0.352	1.409	4.0
B1000		0.353	1.546	4.4	0.352	1.451	4.1
B1050		0.359	1.555	4.3	0.348	1.439	4.1
B1100		0.353	1.570	4.5	0.352	1.559	4.4
C900	Carbon dioxide	0.352	1.391	4.0	0.348	1.423	4.10
C950		0.353	1.391	4.0	0.349	1.402	4.0
C1000		0.350	1.384	4.0	0.351	1.490	4.3
C1050		0.351	1.431	4.1	0.351	1.507	4.3
C1100		0.357	1.648	4.6	0.352	1.515	4.3
H900	Steam	0.352	1.465	4.2	0.348	1.501	4.3
H950		0.353	1.473	4.2	0.346	1.591	4.6
H1000		0.348	1.483	4.3	0.351	1.662	4.7
H1050		0.348	1.510	4.3	0.353	1.563	4.4
H1100		0.355	1.661	4.7	0.349	1.766	5.1

therein, the ACFs derived from PAN fibers have notable adsorption ability.[8,9]

In the development of activated carbons and ACFs, steam and carbon dioxide are commonly used as the activation gases, which create the open pores in the carbon materials. Because the molecular size and reactivity of both activating agents with PAN-based ACFs are different, they lead to different microstructures in the resultant ACFs. In this study PAN-based activated carbon fabrics were developed from continuous carbonization and activation in steam and carbon dioxide at temperatures ranging from 900 to 1100°C. The microstructure changes in the ACFs during different activation processes were studied using wide-angle X-ray diffraction and Raman spectrography. Under these analysis processes, the X-ray diffraction and Raman spectrum were generated only at the fiber surface. Therefore, the samples were analyzed in the original (fabric) and powder forms to examine the surface and inner structures.

EXPERIMENTAL

Oxidized PAN fibers (Toho Rayon Co. Ltd.) were woven into fabrics. The fabrics were 51 mm in width. The oxidized PAN fabrics were carbonized and activated at temperatures from 900 to 1100°C by passing them through a high-temperature oven in a pure nitrogen atmosphere, followed by carbon dioxide and steam. Three groups of carbonized and activated fabrics (samples B, C, and H) were developed using heat-treatment temperatures of 900, 950, 1000, 1050, and 1100°C for 40 min. They were defined as shown in Table I.

An X-ray diffractometer (model 8536 Diano) that provided Ni-filtered Cu Kα radiation was used to measure the crystalline-related properties of the sample. The step-scan method was used to determine the d spacing and stacking size (L_c). The step interval was set at 0.02°. The d spacing and L_c were calculated using eqs. (1) (the Bragg equation) and (2) (the Scherrer equation), respectively:

$$n\lambda = 2d \sin \theta \tag{1}$$

$$L_c(hkl)(\text{nm}) = K\lambda/B \cos \theta \tag{2}$$

in which $\lambda = 0.1542$ nm, K is the apparatus constant (1.0), and B is the half-value width (rad) of the X-ray diffraction intensity (I) versus the 2θ curve.

The Raman spectrometer used here was a Renishaw 2000 instrument with a Raman imaging microscope system, which had the 514.5-nm line of an argon ion laser as the incident radiation.

The samples were analyzed without any treatment or preparation. The scattered light was analyzed using a double-grating monochromator and detected by a cooled photomultiplier tube.

Elemental analysis was carried out with a Perkin–Elmer 240C elemental analyzer. The samples from the carbonization process were analyzed for carbon, hydrogen, and nitrogen. The oxygen content was determined by the differences between these three elements.

The density was measured at 25°C according to the density gradient column method. The density gradient column was prepared with a mixture of *n*-heptane and carbon tetrachloride so that a gradient of about 1.2–1.6 g/mL extended from top to bottom. For the measurement of the density range of 1.6–2.0 g/mL, a density gradient column prepared with a mixture of carbon tetrachloride and 1,3-dibromopropane was adopted.

RESULTS AND DISCUSSION

Under wide-angle X-ray diffraction, PAN fibers demonstrated two main peaks at the $2\theta = 17°$ and 29° positions.[10,11] As the degree of oxidation increased, the structure of the PAN fibers originally at the 17° position gradually disappeared and was replaced by a carbon layerlike (002) structure at around 25°.[12,13] If the fibers were carbonized with a carbonization temperature increasing to about 1000°C, a carbon layer (101) appeared at around $2\theta = 45°$. Because this experiment was in the range of 900–1100°C and the heat-treated fibers were subjected to X-ray diffraction in the form of ground powders We found that almost all of the carbon layerlike structures (002) were at the 25° position, as shown in Figures 1 and 2. Moreover, as the temperature rose a carbon layer (101) structure appeared at $2\theta = \sim 45°$. The results for the *d* spacing of carbon layer structures (d_{002}), the L_c, and the number of layer planes (L_c/d_{002}) are presented in Table I.

The depth of the X-ray diffraction was about 1 μm into the surface of the material. The fiber diameter was about 7–11 μm; therefore, diffraction was generated only at the fiber surface. The structural parameters calculated from the X-ray diffraction in Figure 1 indicated that above 900°C the L_c and L_c/d generally increased in relationship to increases in the treatment temperature, which was due to the linking of the carbon basal plane structures. However, we found that the L_c values of samples C and H, which were subjected to activation treatments at 900–1050°C, were lower than that of sample B. This was because during the activation treatment the water and carbon dioxide reacted with the carbon at the crystal edge or the irregular carbon in the carbon fibers to form carbon monoxide. Among the samples, sample C had the lowest L_c, which was possibly due to the larger molecular size of the carbon dioxide so it could only attack the fiber surface. Because the gaseous water for activation of sample H had smaller molecules, we thought it could permeate into the inner structure of the fibers and mitigate the water molecule attack on the surface. Therefore, the reduction in L_c was not significant. At a temperature of 1100°C the water and carbon dioxide reacted with the crystalline

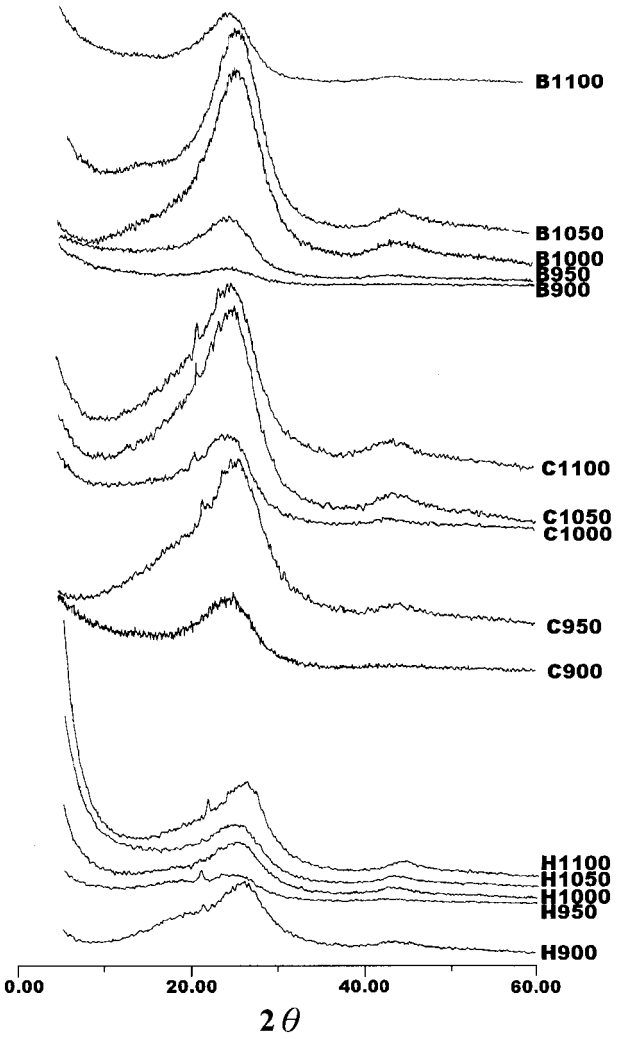

Figure 1 A wide-angle X-ray diffraction pattern of carbon fabric and activated carbon fabrics, which were measured in the fabric form.

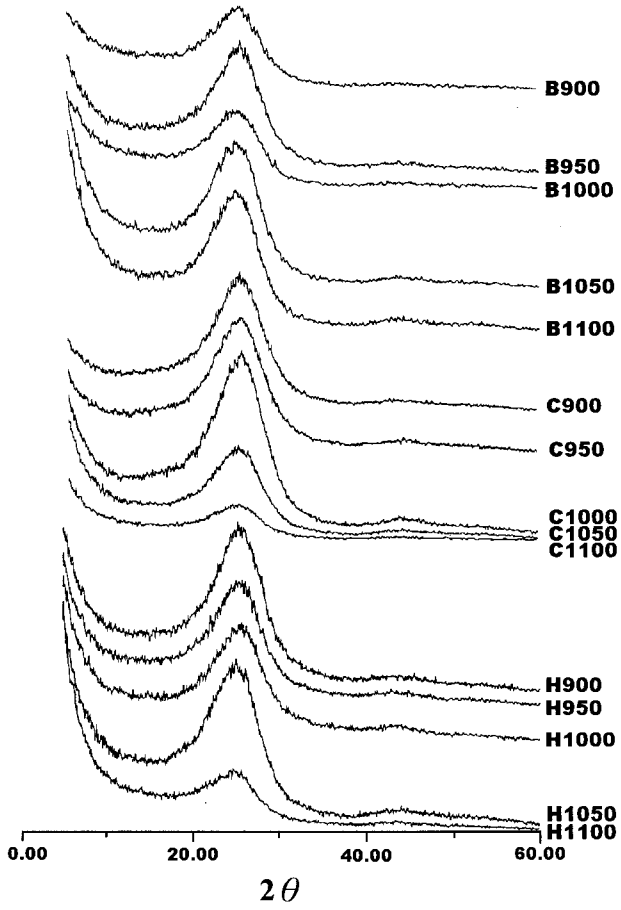

Figure 2 A wide-angle X-ray diffraction pattern of carbon fabric and activated carbon fabrics, which were measured in the powder form.

edges or the irregular carbon on the fiber surface, so the effect of the rise in temperature promoted the interconnection and growth of carbon basal planes structures. These reactions led to a larger L_c in samples C and H over sample B, which formed a more densified surface layer.

In order to verify the above explanations, all samples were further ground into powders, which were then subjected to X-ray diffraction to carry out the analysis on the average overall structure of the activated carbon fabrics. These results are shown in Table I. The data in Table I indicate that the L_c of samples B and C (powder form) were basically the same. This finding suggested that carbon dioxide only reacted with the crystalline edges or the irregular carbon on the fiber surface and that the inner structure of the fibers was not greatly affected.

However, the L_c of sample H (powder form), regardless of the treatment temperature, showed an average overall L_c that was higher than the L_c of samples B and C. When comparing the values of L_c for sample H heated from 900 to 1100°C, the values measured from the powder form were larger than those measured from the fabric form. The values of the powder form increased from 1.50 to 1.77 nm, while the fabric form values increased from 1.47 to 1.67 nm. The L_c increased 17.6 and 13.4%, respectively. This result confirmed the result obtained from the diffraction previously carried out on the carbon fabrics.

The bond lengths of O—H and C═O are 0.096 and 0.121 nm, respectively. The molecular sizes of water and carbon dioxide are around 0.156 and 0.242 nm, respectively. Due to its smaller molecule, water not only reacted with the fiber surface but also easily permeated into the inner structure of the fibers to react with the carbon at the crystal edge or the irregular carbon. Those reactions led to the communicating pore structures on the surface and in the inner portion of the fibers. Such structures facilitated the denitrogenation of the disordered carbon layers in the fibers and the repacking of new carbon basal planes, thus increasing the overall L_c and the L_c/d_{002} in sample H.

The data for the elemental analysis are shown in Table II. As noted in Table II, sample C had a higher nitrogen content than sample B under each of the temperatures. This indicated that there was no extensive denitrogenation and confirmed the X-ray diffraction analysis. Carbon dioxide, which only attacks the fiber surface and

Table II Elemental Composition of Activated Carbon Fabrics (wt %)

Sample Code	N	C	H	O
B900	14.42	81.25	1.61	2.73
B950	11.64	83.61	1.49	3.27
B1000	9.11	86.32	0.91	3.67
B1050	7.64	89.98	0.71	1.68
B1100	6.21	92.03	0.95	0.82
C900	15.27	77.69	1.31	5.74
C950	14.14	81.04	1.24	3.59
C1000	11.26	84.05	0.85	3.85
C1050	8.99	87.70	0.94	2.38
C1100	6.44	91.12	0.69	1.76
H900	9.26	82.89	1.69	6.17
H950	7.46	86.74	1.34	4.47
H1000	6.91	88.37	1.25	3.48
H1050	4.83	90.45	0.90	3.83
H1100	5.07	90.86	1.12	2.96

cannot penetrate the inner structure of the fibers to produce internally and externally communicating pore structures, did not promote denitrogenation in the fibers, which led to a decrease in the mean L_c. In contrast, the nitrogen content of sample H under each temperature was much lower than that of samples B and C and thus more denitrogenation reactions occurred therein. This result further verified the X-ray diffraction analysis.

The results in Table II indicate that as long as the activated carbon fabrics had undergone activation, the oxygen content of samples C and H was higher than that of purely carbonized fabrics under the same treatment temperature. The oxygen content of the samples during heat treatment was in the order of sample H > sample C > sample B. This was probably caused by the generation of more oxygen-containing functional groups during the activation process. If the type of surface functional groups is to be further analyzed, it is necessary to conduct an ESCA surface analysis.

The Raman laser spectrum analysis generally suggested that, because the carbon atoms had three types of electron hybridized orbitals, a few allotropes were formed. It was also generally suggested that the inner structure of the carbon composition of the phenolic type was a carbon layer structure formed by the C═C bond of sp^2 (graphite structure) for the most part and the C≡C bond of sp^3 in fewer numbers. The release of noncarbon elements and the different degree of carbonization in the carbonization process led to differences in the L_c of the entire block. The types of carbon bonding were analyzed using a Raman laser spectrum from which the degree of order of the L_c could be analyzed. In the region of Raman scattering analysis, the C—C bond of the sp^3 hybridized orbital formed a fairly strong characteristic peak at 1332 cm^{-1}.[14–16] The C═C bond of the sp^2 hybridized orbital had a characteristic peak at 1582 cm^{-1} (the so-called G mode, which is formed by the ordered region in the carbon layers). Moreover, there were two secondary characteristic peaks (the so-called D mode, which is caused by the disordered part in the carbon layers) at 1357 and 1620 cm^{-1}. There was also a characteristic peak caused by the noncrystalline carbon in the region between about 1500 and 1550 cm^{-1}.[15,17–19] It is now generally accepted that the dependence between the integrated intensity ratio I_D/I_G and the microcrystalline planar crystal size L_a shows inversely proportional behavior. Furthermore, the equation by Tuinstra and Koenig,[20]

$$L_a = 44 \times (I_D/I_G)^{-1} \quad (3)$$

may be used to obtain the mean microcrystalline planar crystal size, wherein I_D and I_G are the integral area of the D and G modes, respectively.

Curve fitting was carried for all samples. The best fitting was invariably obtained for all samples with two Lorentzian lines at around 1360 and 1600 cm^{-1} and a broad Gaussian band at about 1540–1550 cm^{-1}. Figures 3–5 show the Raman spectrum analytical diagrams of activated carbon fabrics subjected to different activation treatments. Table III shows the results calculated after the curve fitting of Figures 3–5, wherein each sample was classified into two major parts: the fabric form and the powder form.

For sample C the Raman analysis performed on the activated carbon fabrics revealed that the L_a value for sample C was even smaller than that for sample B. This was because the carbon dioxide molecules were larger and could thus easily and continuously attack the crystalline edges of the carbon layer or the nonregular carbon part of the fiber surface, which caused the fiber surface to have larger pores. As the treatment temperature increased this reaction also promoted the growth of carbon layers.

However, when the analysis was directed to the pulverized activated carbon fabrics of sample C, we found that under the same treatment temperature the L_a of the carbon layer planes was larger than that of sample B (powder form) and sample C (fabric form). This was because the carbon dioxide molecules, while primarily act on the fiber surface, produced pores on the surface that more or less promoted the denitrogenation of the fiber subsurface and progressive growth of carbon basal planes in the fibers. It was not easy for denitrogenation to occur inside the fibers of sample B, which led to the disordered structure inside the fibers, because the B group had a denser fiber surface than sample B. Therefore, sample C generally had a higher L_a than samples B and C in the fabric form.

In regard to sample H in its fabric form, the Raman analysis on the activated carbon fabrics ascertained that the L_a value was larger than that in sample B in the temperature range of 950–1100°C. The reason was the smaller size of the water molecules, which easily penetrated and

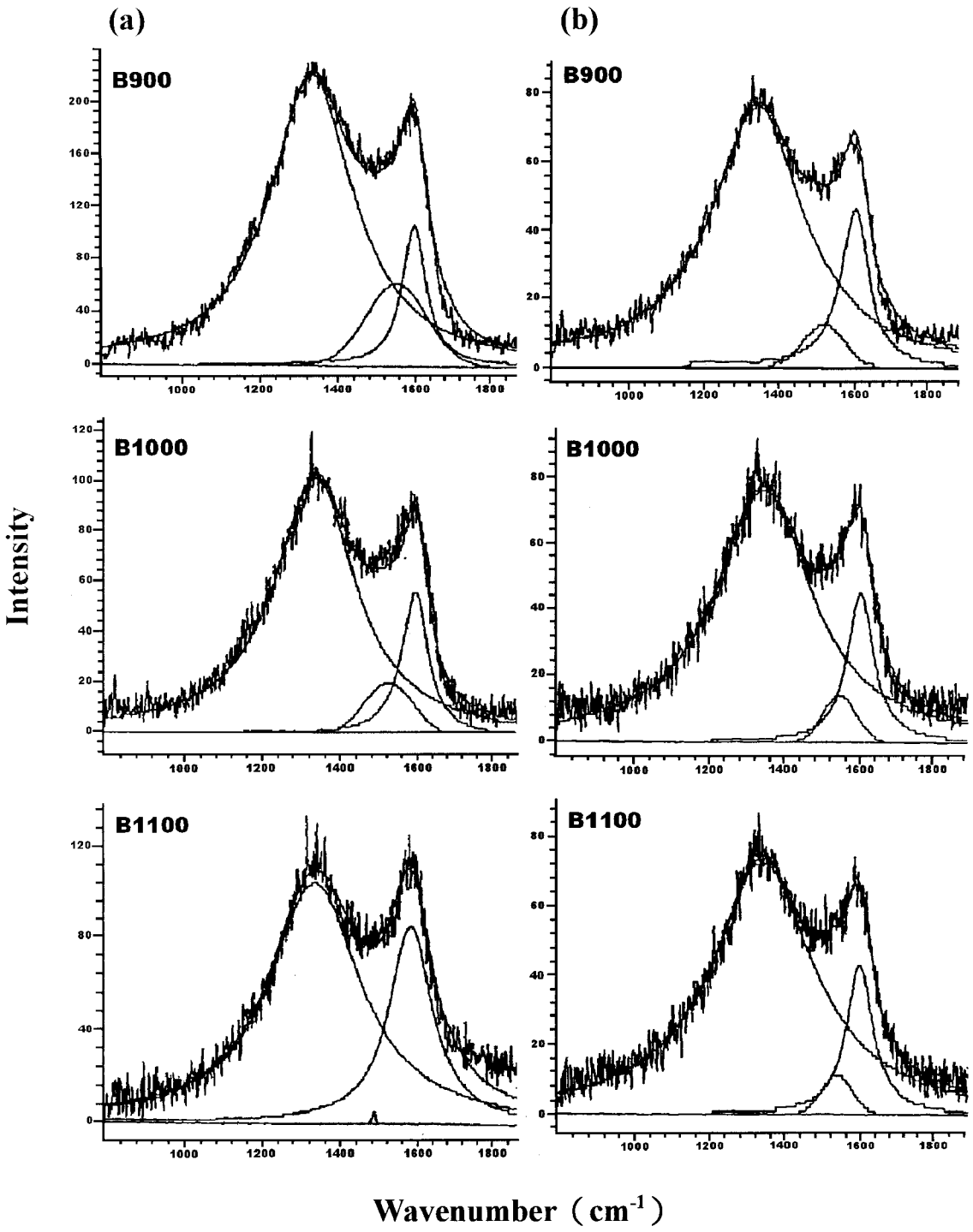

Figure 3 Raman spectra of carbon fabrics after pyrolysis, which were measured in (a) fabric and (b) powder forms.

reacted with the inside of the fibers. The water molecules reacted not only on the fiber surface but also with the carbon at the crystal edge or the nonregular carbon in the fibers. Consequently, the L_a of the fiber surface of sample H was larger than that of samples B and C.

The analysis of the pulverized activated carbon fabrics of sample H showed that the L_a was likewise larger than that in samples B and C and the surface of sample H. This was because water molecules easily penetrated to the inside structure of the fibers to react with the carbon at the crystal

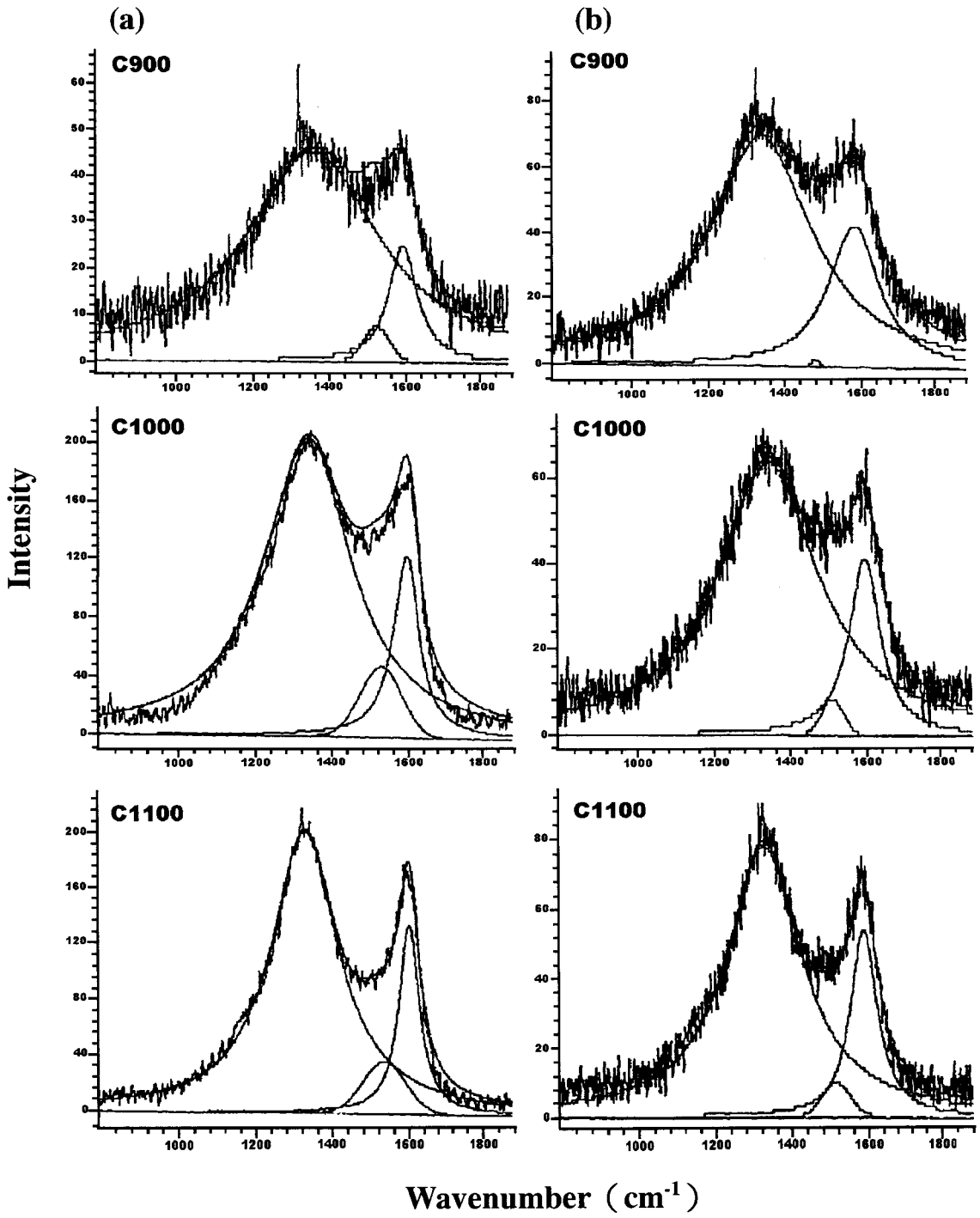

Figure 4 Raman spectra of carbon dioxide activated carbon fabrics after pyrolysis, which were measured in (a) fabric and (b) powder forms.

edge or the nonregular carbon. This reaction led to the linking of micropores on the fiber surface with the internal pores. Therefore, the L_a of sample H would generally be larger than that of sample B. However, the fibers activated with steam or carbon dioxide, when compared with purely carbonized fabrics, had increased L_a values (on the fiber surface or in the fibers). In addition, above 1000°C the area ratio of the integral strength (I_D/I_G) of samples C and H (powder form) was

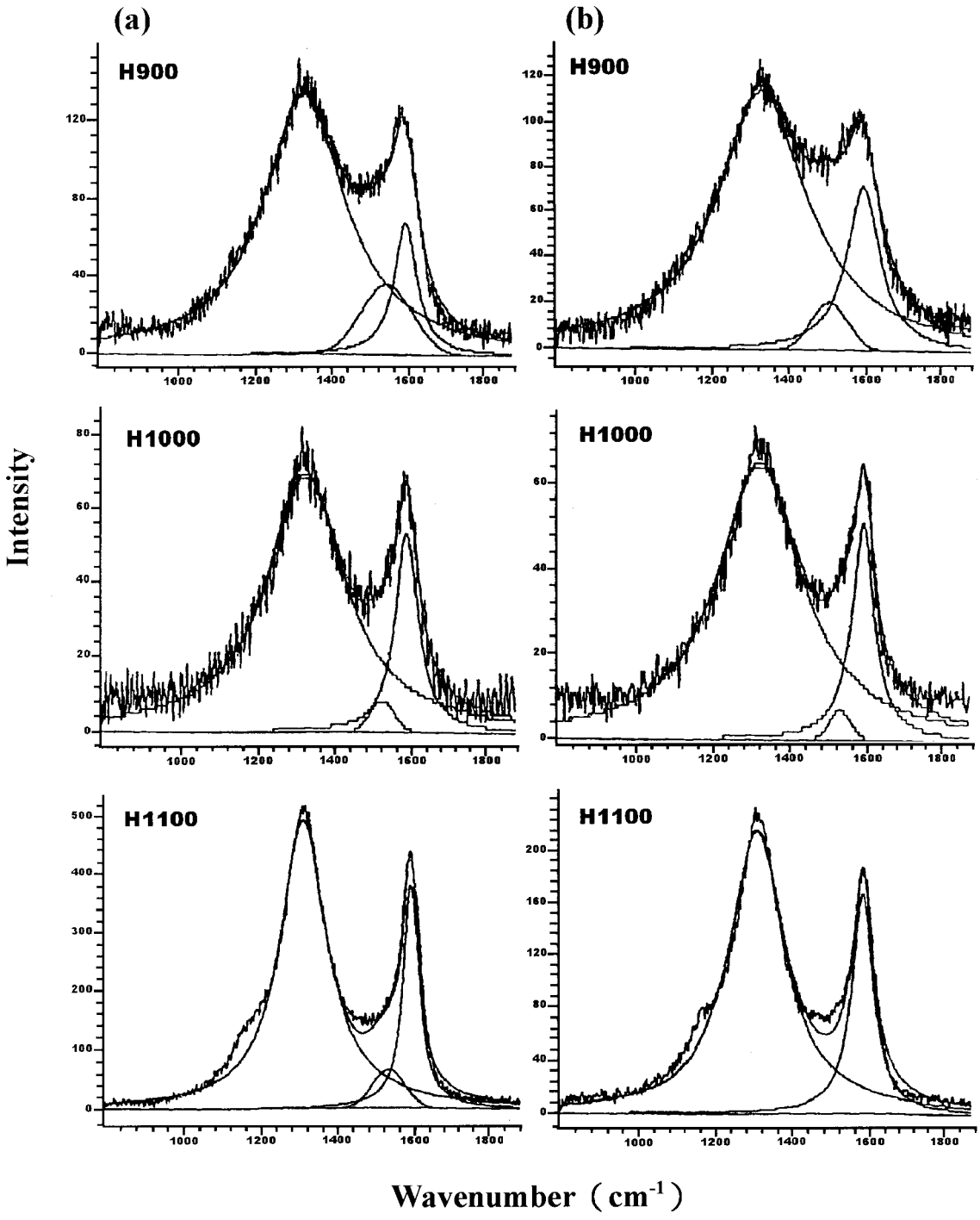

Figure 5 Raman spectra of steam activated carbon fabrics after pyrolysis, which were measured in (a) fabric and (b) powder forms.

found to be smaller than sample B (powder form), which was carbonized at the same treatment temperature, regardless of the type of activation conditions (Table II). This finding indicated that activated carbon fabrics had a more ordered structure in the carbon layers compared with the purely carbonized fabrics. This was because during activation the gas reacted with the crystalline edges of the carbon layer or the irregular carbon in the fibers.

Table III Analysis of Raman Spectra from Carbon Fabrics and Activated Carbon Fabrics

	Sample Form			
	Fabric		Powder	
Sample Code	I_D/I_G	L_a (nm)	I_D/I_G	L_a (nm)
B900	7.06	0.62	6.49	0.68
B950	6.59	0.67	6.70	0.66
B1000	5.48	0.80	6.48	0.68
B1050	4.89	0.90	6.26	0.70
B1100	2.54	1.73	6.24	0.71
C900	8.19	0.54	4.96	0.89
C950	6.89	0.64	4.98	0.88
C1000	5.50	0.80	5.11	0.86
C1050	5.39	0.82	5.21	0.84
C1100	4.98	0.90	4.22	1.04
H900	7.37	0.60	4.44	0.99
H950	5.15	0.80	5.16	0.85
H1000	4.71	0.93	4.68	0.94
H1050	4.64	0.95	4.30	1.02
H1100	3.87	1.14	3.37	1.30

Figure 6 shows the variations in the densities of each sample under different treatment temperatures. The largest density value for sample B was obtained at 900°C. This was due to the crosslinking among the ladder polymer structures in the oxidized fibers and the loss of small molecules during the carbonization process, which gradually led to the formation of a graphitelike structure and a denser fiber structure. Above 900°C the density of the carbonized fabric decreased with the increase in the carbonization temperature. Moreton and Watt[21] proposed that the impurities present inside the fibers caused the generation of defects and pores on the fiber surface during carbonization. When the carbonization temperature was above 800°C, graphitelike structure packing occurred and the direction of growth became perpendicular to the fiber axis. Because of the linking of the carbon basal planes caused by denitrogenation, the pores in the fibers were converted from open to closed pores, leading to a drop in the fiber density. With the confirmation of the Raman laser spectrum analysis that the L_a of sample B increased with a rise in temperature, it was thus speculated that open pores on the fiber surface were converted into closed pores, which lowered the fiber density.

In sample C the rate of diffusion of carbon dioxide into the pore system of the block was slower because of the larger carbon dioxide molecular size. This restricted the formation of micropores. Moreover, carbon dioxide reacted with the crystal edge or the irregular carbon on the fiber surface, which impeded the conversion of open pores into closed pores. Also, the extent of the activation reaction increased as the temperature increased, which led to an increase in the number of pores. The densities obtained at any treatment temperature above 950°C were higher than that of sample B. At 900°C the density of sample C was lower than that of sample B. This was perhaps due to the lower reaction temperature. It caused a poorer activation effect and the removal of only some irregular regions of fibers, leading to a densified structure.

In sample H the density was lower than that of sample B at 900°C. The reason for this was similar to that of sample C: it was probably caused by the lower reaction temperature. However, the densities at each treatment temperature above 950°C were all higher than 2 g/mL. At 1050°C the density of sample H increased to 2.28 g/mL. This was because the water molecules were smaller and easily penetrated into the fibers, which led to the linking of the internal and external pore structures and thus the considerable rise in density. Calculations from the Raman laser spectrum analysis indicated that sample H had a larger L_a than the others. We surmised that water would have a violent reaction with the fibers at 1100°C and attack not only the crystal edges or the irregular carbon region, but also may have further

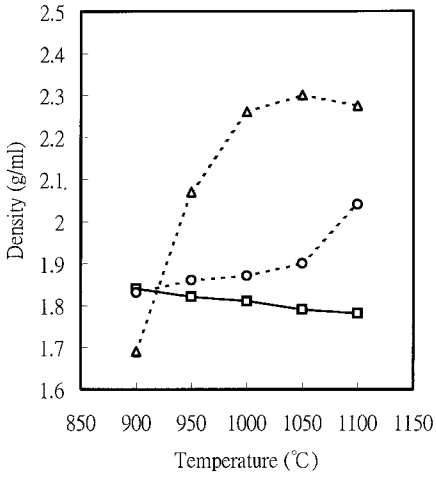

Figure 6 The variation of the density of resulting carbon fabric and activated carbon fabrics as a function of the carbonization temperature for (□) sample B, (○) sample C, and (△) sample H.

reacted with the crystalline carbon layers, thus causing a decrease in the fiber diameter and weight. Although the fiber surface would peel off, denitrogenation of the carbon layer inside the fiber and crosslinking reactions would be provided at the same time, which would increase the L_a and lead to a reduction in open pores and a drop in density.

CONCLUSIONS

Steam and carbon dioxide developed the microstructure initially present in PAN-based activated carbon fabrics, but with different effects. These fabrics in the form of fabric and powder were examined by X-ray diffraction and Raman spectrography. This study indicated that carbon dioxide only reacted with the crystalline edges or the irregular carbon on the fiber surface and that the inner structure of the fibers was not greatly affected. When carbon fabrics were activated using steam, water molecules reacted not only on the fiber surface but also with the carbon at the crystal edge or the irregular carbon in the fibers, which led to communicating pore structures on the surface and in the inner portion of the fiber. Those reactions promoted the denitrogenation reactions occurring therein and the formation of oxygen-containing functional groups. Because of these structures and reactions, these activated carbon fabrics had the highest L_c, the highest L_c/d_{002}, the highest oxygen content, the largest L_a, the highest density, and the lowest nitrogen content over other samples.

Our financial support is gratefully acknowledged.

REFERENCES

1. Arons, G. N.; Machair, R. N. Text Res J 1974, 42, 60.
2. Lin, R. Y.; Economy, J. Appl Polym Symp 1973, 21, 143.
3. Economy, J.; Lin, R. Y. U.S. Pat. 3,769,144, 1973.
4. Economy, J.; Lin, R. Y. U.S. Pat. 3,831,760, 1974.
5. Economy, J.; Lin, R. Y. J Mater Sci 1971, 6, 1151.
6. Ko, T. H.; Chiranairadul, P.; Lu, C. K.; Lin, C. H. Carbon 1992, 30, 647.
7. Ko, T. H.; Chiranairadul, P.; Lin, C. H. Polym Eng Sci 1991, 31, 1618.
8. Ikegmi, S. L.; Hirai, M.; Izumi, K. U.S. Pat. 4,362,646, 1980.
9. Ikegmi, S. L.; Hirai, M.; Izumi, K. U.S. Pat. 4,412,937, 1983.
10. Wallner, L. G.; Riggert, K. J Polym Sci 1963, B1, 111.
11. Klement, J. J.; Geil, P. H. J Polym Sci 1968, A2, 1381.
12. Ko, T. H.; Ting, H. Y.; Lin, C. H. J Polym Sci 1988, 35, 631.
13. Ko, T. H.; Ting, H. Y.; Lin, C. H. J Polym Sci 1989, 37, 553.
14. Colvin, B. G.; Storr, P. Eur Polym J 1974, 10, 337.
15. Knight, D. S.; White, W. B. J Mater Res 1989, 4, 385.
16. Lespade, P.; Marchand, A.; Couzi, M.; Cruege, F. Carbon 1984, 22, 374.
17. Robertson, J. Adv Phys 1986, 35, 317.
18. Nikiel, L.; Jagodzinski, P. W. Carbon 1993, 31, 1313.
19. Huong, P. V. Diamond Rel Mater 1991, 1, 33.
20. Tuinstra, F.; Koenig, J. L. J Chem Phys 1970, 53, 1126.
21. Moreton, R.; Watt, W. Carbon 1974, 12, 543.